THE JOURNAL OF PHYSICAL CHEMISTRY A

Article

pubs.acs.org/JPCA

Protein Attachment on Nanodiamonds

Chung-Lun Lin,[†,‡] Cheng-Huang Lin,[‡] Huan-Cheng Chang,*[,†] and Meng-Chih Su*[,§]

[†]Institute of Atomic and Molecular Sciences, Academic Sinica, 1 Sec. 4, Roosevelt Rd., Taipei, Taiwan 10617, R.O.C

[‡]Department of Chemistry, National Taiwan Normal University, 88 Sec. 4, Ting-Chow Rd., Taipei, Taiwan 11677, R.O.C

[§]Department of Chemistry, Sonoma State University, 1801 E. Cotati Ave., Rohnert Park, California 94928, United States

Supporting Information

ABSTRACT: A recent advance in nanotechnology is the scale-up production of small and nonaggregated diamond nanoparticles suitable for biological applications. Using detonation nanodiamonds (NDs) with an average diameter of ∼4 nm as the adsorbents, we have studied the static attachment of three proteins (myoglobin, bovine serum albumin, and insulin) onto the nanoparticles by optical spectroscopy, mass spectrometry, and dynamic light scattering, and electrophoretic zeta potential measurements. Results show that the protein surface coverage is predominantly determined by the competition between protein−protein and protein−ND interactions, giving each protein a unique and characteristic structural configuration in its own complex. Specifically, both myoglobin and bovine serum albumin show a Langmuir-type adsorption behavior, forming 1:1 complexes at saturation, whereas insulin folds into a tightly bound multimer before adsorption. The markedly different adsorption patterns appear to be independent of the protein concentration and are closely related to the affinity of the individual proteins for the NDs. The present study provides a fundamental understanding for the use of NDs as a platform for nanomedical drug delivery.

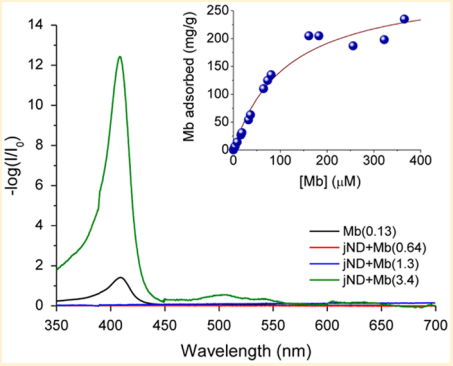

INTRODUCTION

Nanotechnology is an enabling technology with wide-ranging applications. The convergence of this technology with molecular biology has opened up many new avenues in the fields of drug delivery, cancer therapy, diagnostic imaging, and biosensing, etc.[1,2] Recently, there has been a growing interest in the use of carbon-based nanomaterials, including fullerenes,[3] nanotubes,[4] graphene,[5] and nanodiamonds (NDs),[6,7] for biotechnological and biomedical applications. Cytotoxicity tests with various cancer cell lines indicate that NDs are the least toxic of all carbon nanoparticles presently studied.[8] These biocompatible particles have a multitude of potential applications as gene and drug delivery vehicles,[9] optical contrast agents,[10] and nanoscale sensors.[11]

Prevailing NDs can be roughly separated into two groups according to their methods of synthesis: high-pressure-high-temperature NDs (HPHT-NDs) and detonation NDs (DNDs).[12] The former are produced by the crushing or ball-milling of micron-sized diamond particles synthesized with HPHT presses. Although their size distribution is broad (typically 30−100 nm), they are monocrystalline and can be readily purified by air oxidation and strong acid washes. The later, on the other hand, are synthesized by shock wave compression using explosive compounds such as TNT and RDX. With proper explosive mixture ratios, the shock wave can produce DNDs with a remarkably narrow particle size distribution of 4−5 nm in diameter for the primary particles. Elaborate postprocessing deagglomeration, however, is required to break the covalent linkage between disordered (sp^2) carbon atoms on their surfaces. Osawa has provided a complete account of the methods for fabricating deagglomerated DNDs with wet ball milling techniques.[13]

This work aims to make a comparative study of the attachment of proteins to these two types of NDs. A number of studies have shown that HPHT-NDs, after washes with strong oxidative acids, can bind noncovalently but strongly with proteins through the combination of electrostatic force, hydrogen bonding, and hydrophobic interactions.[14] These particles are negatively charged and useful as solid-phase extraction supports for proteomic analysis.[15] Additional experimental evidence shows that HPHT-NDs surface-coated with bovine serum albumin have a high dispersibility in biological buffers such as phosphate-buffered saline, a feature of particular importance in biolabeling applications.[16] Whether these unique characteristics are preserved in DNDs is an interesting question to address, since the changes in size, shape, and surface properties can significantly affect the binding affinity of the carbon nanoparticles for proteins.

Special Issue: 100 Years of Combustion Kinetics at Argonne: A Festschrift for Lawrence B. Harding, Joe V. Michael, and Albert F. Wagner

Received: January 31, 2015
Revised: March 20, 2015

DOI: 10.1021/acs.jpca.5b01031
J. Phys. Chem. A XXXX, XXX, XXX−XXX

Ho and co-workers were the first to apply deagglomerated DNDs as drug, protein, and gene delivery vehicles.[9] These nanometric particles are monodispersed and positively charged at neutral solution pH. They are appealing for such applications because their surfaces can be readily conjugated with bioactive ligands and possess a high loading capacity per weight as well as a functional mechanism for targeted release. It has been demonstrated that the deagglomerated DNDs can play a significant role in the therapeutic release of proteins like insulin[17] and transforming growth factor beta (TGF-β).[18] Specifically for ND-delivered insulin, it can serve as a potential promoter of wound healing and vascularization in patients with severe burns and other conditions. Interestingly, the ND delivery of insulin is pH-triggered, thereby allowing for the use of this method to target bacterial infections accompanying serious wounds. The present study is designed to provide a fundamental understanding of these intriguing phenomena and to elucidate in detail the nature of how different types of proteins (such as bovine serum albumin, myoglobin, and insulin) interact with these nanoparticles by optical spectroscopy[19−21] and mass spectrometry.[14,15]

EXPERIMENTAL SECTION

Chemicals. Bovine serum albumin (BSA), horse heart myoglobin (Mb), human insulin (Ins), 2,5-dihydroxybenzoic acid (DHB), trifluoroacetic acid (TFA), and all other chemicals were obtained from Sigma-Aldrich and used without further purification.

Materials. Synthetic HPHT diamond powders (MSY 0−0.05) and aqueous DND colloids (NanoAmando) were obtained from Microdiamant (Switzerland) and New Metals & Chemicals (Japan), respectively. The HPHT-NDs were purified by air oxidation at 450 °C for 1 h and then treated in concentrated H_2SO_4−HNO_3 (3:1, v/v) solution at 100 °C in a microwave reactor (Discover BenchMate, CEM) for 3 h. The NanoAmando, consisting of dispersed DND particles (concentration: 5%, size: 3.7 nm) in water after optimized deagglomeration, was used as received. A particle size and zeta-potential analyzer (Delsa Nano C, Beckman-Coulter) characterized the size distributions and surface charge states of these NDs and their bioconjugates in distilled deionized water.

Sample Preparation. NDs (10 mg/mL for DNDs and 1.0 mg/mL for HPHT-NDs) were mixed with BSA, Mb, and Ins separately. Prior to the mixing, concentrations of the stock sample solutions were measured by using the molar extinction coefficients of the individual proteins. To facilitate protein adsorption onto NDs through electrostatic forces, pH values of the mixed sample solutions were adjusted for the individual proteins by adding diluted NaOH or HCl. After sonication for 5 min in ice water and subsequent shaking for 5 min at room temperature, protein-attached NDs in the mixtures were separated by centrifugation with an ultracentrifuge (CS150GXL, HITACHI) at 55000 rpm for 1.5 h. The supernatants were collected for optical spectroscopic analysis. The precipitates were then washed with deionized distilled water to remove unbound protein molecules, and the resulting mixtures were shaken for 10 min before another centrifugation at 55000 rpm for 1.5 h. The final precipitates were collected for mass spectrometric analysis.

UV−vis Absorption Spectroscopy. Concentrations of proteins in the supernatants were determined by measuring the light intensity ratios (I/I_0) between the sample and reference beams over 200−800 nm using a UV−vis spectrophotometer (U-3310, Hitachi). The amounts of the proteins attached to the NDs were calculated from the concentration differences before and after protein adsorption in water. Due to the strong light scattering from NDs, the spectra were plotted as $-\log(I/I_0)$ (instead of absorbance) against wavelength.

Matrix-Assisted Laser Desorption/Ionization Time-of-Flight Mass Spectrometry (MALDI-TOF MS). Proteins or protein−NDs were mixed with saturated DHB dissolved in acetonitrile/H_2O solution (v/v = 2:1) containing 0.1% TFA for MALDI plate spotting. Positive ion MS spectra were acquired with a reflection TOF mass spectrometer (Microflex, Bruker-Daltonics) for either the proteins alone or the protein−ND complexes, following procedures described previously.[14,15]

RESULTS AND DISCUSSION

Three proteins were used to study their static attachment on two different types of NDs: jND (i.e., DNDs with positive surface charges and manufactured by the Osawa group in Japan)[22] and hND (i.e., HPHT-NDs with negative surface charges and made in this group).[14] Additional effort was made to keep both NDs from forming aggregates and, ultimately, achieving the protein attachment on a nearly single ND platform. The three chosen proteins were: Mb, BSA, and Ins, each representing a unique surface attachment on ND as described in the following sections.

NDs are known to form aggregates, regardless of the types of the surface charges that they may have carried. Thus, it has been a challenge for researchers to keep the size of the NDs small and well-defined when a ND is used as a platform to grow proteins on its surface. ND aggregates of random sizes will directly affect protein surface coverage, among others, presenting various difficulties in quantifying the protein−surface interactions. Therefore, small and individual NDs are desired for the surface attachment studies. Osawa's recent effort in making stable and nonaggregated DNDs of ca. 4−6 nm diameter proves ideal for this work. Some preliminary testing was carried out first to determine the stability of jND, both in terms of the time duration and pH changes, as separated nanoparticles for this study. The experimental conditions used for each protein reported here have all tested satisfactory in providing predominantly individual jNDs of the particle size approaching the single particle limit. In comparison, the size of hNDs is about 6 times as large, averaging 30 nm in diameter as routinely tested in this lab.[23]

Myoglobin + ND. Mb is a globular protein with a crystallographic size of 2.5 × 3.5 × 4.5 nm^3.[24] The protein has an isoelectric point (pI) of ∼6.9 and at pH 7.5, it favors electrostatic attachment on a positively charged surface such as jND. The surface interaction of Mb with jND is characterized by the Soret absorption (at 409 nm) of its heme group using UV−vis spectroscopy. Figure 1 displays the Soret absorption from the supernatant of Mb + jND solutions at pH 7.5 in increasing Mb concentration. The absorption of the Mb stock solution (0.13 mg/mL or 7.6 μM) is also included for comparison, which will be used for deriving the Langmuir isotherms. Protocols for the spectroscopic measurement are similar to our previous study of cytochrome c with hND.[19] The concentration of jNDs was fixed at [jND] = 10 mg/mL for all sample solutions. Notably, this high jND concentration is required to keep jND from aggregation, according to the manufacturer's instruction and the tests in this work. The [Mb] varied from 0.03 to 6.3 mg/mL, covering a range of two orders-of-magnitude change from under to well-beyond surface

DOI: 10.1021/acs.jpca.5b01031
J. Phys. Chem. A XXXX, XXX, XXX−XXX

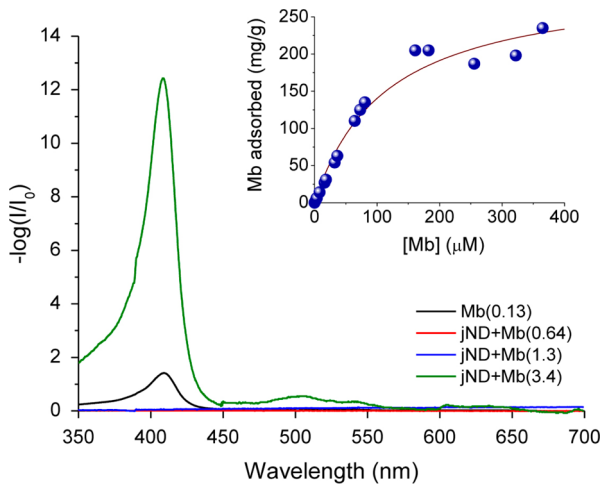

Figure 1. UV−vis absorption spectra of Mb stock (0.13 mg/mL) and Mb + jND supernatant for [Mb] = 0.64, 1.3, and 3.4 mg/mL (numbers in parentheses) in 10 mg/mL jND at pH 7.5. (See text.) Inset: Adsorption isotherm of Mb on jND at pH 7.5. Solid curve is the best fit from the Langmuir adsorption model (eq 1 in text). Appropriate dilution of the supernatant was made to obtain the spectra with $-\log(I/I_0) < 2$ in measurement.

saturation. Some samples in Figure 1 show measurable absorption signals from the Soret band, presumably caused by free Mb left in the supernatant solution, of which the band intensity increases as a function of [Mb]. Other samples show no measurable Soret absorption, suggesting an under-saturated surface coverage with all Mb attached on jND. No sign of surface-bound Mb was found in the supernatant. This assessment is based on the fact that in the figure, both the Soret peak position and band shape remain unchanged in all collected spectra. Additional evidence comes from the dynamic light scattering (DLS) measurement, which shows no Mb + jNDs detectable in the supernatant, consistent with the UV−vis finding.

Consequently, an equilibrium is established between free Mb in the supernatant, $Mb_{(aq)}$, and surface-bound $Mb_{(s)}$ on the ND: $Mb_{(aq)} \rightleftharpoons Mb_{(s)}$. The associated surface adsorption constant, K_a, can be determined by the study of adsorption isotherms following the method developed in our previous work.[19] The experimental data fit reasonably well to the isotherm equation of Langmuir's surface adsorption model,

$$\Theta = \frac{K_a C_b}{1 + K_a C_b} \quad (1)$$

where Θ is the ratio between the occupied surface sites and the total available sites (when Θ = 1, the surface is saturated) and C_b is the protein concentration in each sample solution. The inset in Figure 1 shows the derived isotherm for Mb + jND at pH 7.5 with a fitted $K_a = 8.8 \times 10^3\ M^{-1}$. The value is nearly two orders-of-magnitude less thermodynamically favorable than that of Mb + hND at pH 5.0, where electrostatic forces also play a major role in the protein attachment (see ref 14 and also Figure S1 of the Supporting Information). It is noted that the size of Mb (~4 nm) is about the same as jND (~4 nm) but much smaller than that of hND (~30 nm). The latter has a considerably larger surface area per particle, which could enhance the stability in protein−surface interactions. As will be discussed later, the characteristic of the weak protein−surface interaction and the low loading capacity of jND allow us to reveal some unique protein−protein interactions upon attachment on NDs.

Next, we address the question about the formation of the protein−ND complex: has Mb successfully attached to the ND? Electrophoresis experiments were thus carried out to determine the zeta potential of Mb with jNDs. Figure 2a shows the zeta

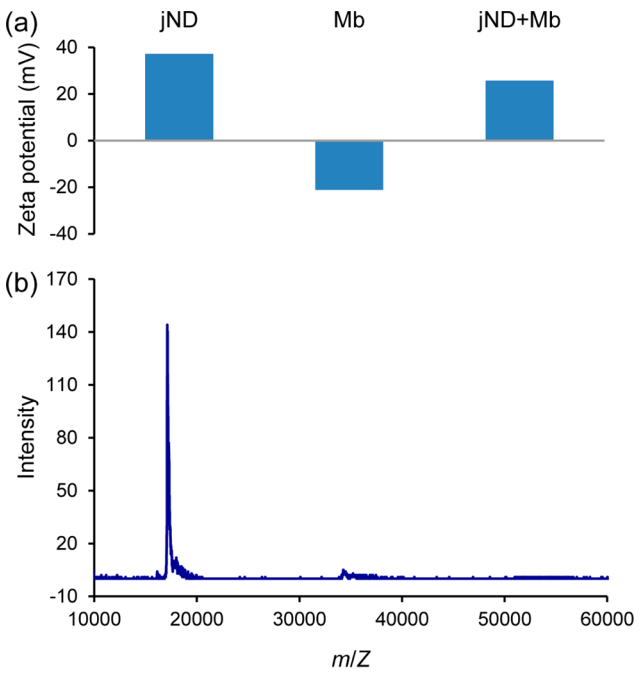

Figure 2. (a) Zeta potential measurements of Mb, jND, and Mb + jND at pH 7.5. (b) MALDI-TOF mass spectrum of Mb + jND. The protein−ND complex sample was prepared with [Mb] = 2.0 mg/mL in 10 mg/mL jND.

potentials measured from jND, Mb, and Mb + jND to be +37.2, −21.2 and +25.7 mV, respectively. The positive potential of jND is attributed to its positive surface charge, which has a relatively high value, suggesting good stability in the ND's individual particle form. The lowering of the positive potential in Mb + jND is evidence of the coupling through a static interaction between the two. The smaller zeta potential indicates an increase in the interparticle interactions between neighboring complex molecules, leading to the formation of aggregates. This is expected to become more significant when the protein concentration is raised higher.

More details of the surface coverage are provided by the MALDI-TOF MS study of the protein−ND complex. As previously demonstrated,[14,15] the method serves as an effective means to characterize the protein attachment on NDs without the need of preseparation. In this experiment, the complex sample was prepared by centrifuging the sample solution after it has been well-mixed. Supernatant was decanted and washed and then centrifuged again. The precipitated sample went through MALDI followed by TOF sorting for the fragmentation pattern. Any distinct mass signal obtained must have come from the surface-bound Mb since ND does not have a well-defined mass. One major mass peak from the Mb + jND complex appears at 17120 Da (Figure 2b), corresponding to the molecular mass of Mb, which accounts for >99% of the total intensity on the mass spectrum. Only trace amounts of the Mb-dimer can be located at two times of mass away from the parent peak, similar to that of Mb + hND (Figure S2 of the

DOI: 10.1021/acs.jpca.5b01031
J. Phys. Chem. A XXXX, XXX, XXX−XXX

Supporting Information). Given the molecular mass of 17 kDa for Mb and ~62 kDa for jND (assuming spherical with a diameter of ~3.7 nm),[13] the saturated surface coverage of ~0.25 g/g (inset in Figure 1a) suggests that the Mb-jND predominantly forms a 1:1 complex at saturation. The adsorption of Mb onto jND follows

$$\text{protein} + \text{jND} \rightleftharpoons \text{protein}\cdot\text{jND} \quad (2)$$

Is this expression generally applicable to other proteins? To address this issue, we studied the adsorption of BSA and insulin on jNDs.

BSA + ND. Unlike Mb, which is nearly spherical in shape, BSA is a prolatelike ellipsoid with a diameter of 4 nm and a length of 14 nm.[25] It has a pI ~ 4.7 and a molecular mass of 66 kDa, close to that of jND. How it binds with jND, which is smaller in size, and the resulting stereochemistry deserve close examination. Previously, we have studied the BSA attachment on 100 nm hND over pH 3–9 and determined a protein loading capacity of ~150 mg/g at pH 5.5.[14] It suggests that more than 60 BSA molecules can be attached to each 30 nm hND particle. For BSA + jND, the experiments were maintained at pH 5.5 to maintain good dispersibility and achieve necessary surface attraction. Again, with the jND concentration fixed at 10 mg/mL, the BSA concentration range was chosen to sufficiently cover from under to over surface saturation on jND. Figure 3 shows UV–vis absorption spectra

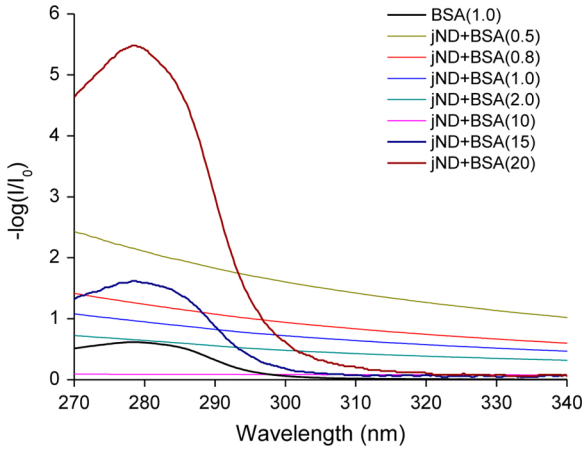

Figure 3. UV–vis absorption spectra of BSA stock (1.0 mg/mL) and BSA + jND supernatant for [BSA] = 0.5–20 mg/mL (numbers in parentheses) in 10 mg/mL jND at pH 5.5. (See text.) Appropriate dilution of the supernatant was made to obtain the spectra with $-\log(I/I_0) < 2$ in measurement.

of BSA + ND samples at different [BSA] ranges. At [BSA] = 0.5–10 mg/mL, or the number ratio of BSA/jND = 0.5–10, respectively, only the scattered light from free jND in the supernatant is detected at the wavelength range of 270–340 nm. The up-tilting of the signals toward the far UV region is a result of the strong light scattering from the residual jNDs, whose intensity is inversely proportional to the fourth powers of light wavelength.[26] The intensity decreases as the protein concentration increases (top down in Figure 3), suggesting that an increase of the protein content in the sample has effectively removed the jND from the solution. Zeta potential measurements for free jND, free BSA, and BSA + jND indeed support the observations. The relatively high values of the potentials (in both polarities) for jND and free BSA at +33.2 and −28.5 mV, respectively, favor the nonaggregated state. The BSA + jND has a potential of +15.2 mV, which is reduced in half from the zeta potential of free jND. Similar to the case of Mb described in the previous section, this new potential is significantly different from either jND or free BSA, representing the presence of a new BSA + jND complex form.

As the BSA concentration continues to increase (from the bottom up in Figure 3), a spectral feature around 280 nm begins to grow, which is the known absorption feature of tryptophan in BSA. In the same figure, an absorption spectrum of stock BSA is also included to verify the band shape and location of the growing feature. It is therefore concluded that the absorption signals at ~280 nm in Figure 3 are all due to free BSA in supernatant. Apparently, the jND surface is already saturated for the samples with [BSA] = 15 mg/mL. In finding the number ratio at the saturation point, we trace the onset of the appearance of the BSA absorption band in the UV–vis spectra and locate the surface saturation at 11 mg/mL BSA with 10 mg/mL jND, which gives a maximum occupancy of BSA/jND ~ 1. Hence, similar to Mb, a proposed reaction scheme for BSA on jND can then be described by an equilibrium established between BSA in solution and on the jND surface as BSA + jND ⇌ BSA·jND. MALDI-TOF spectra for BSA + jND were also obtained, which show only the parent peak within the mass-to-charge scale of our mass spectrometer (data not shown). The large molecular mass of BSA excludes the possibility of observing multimers in the mass spectra.

Insulin + ND. Insulin has a pI of ~5.4 and a molecular mass of 5.8 kDa, which is about one-tenth that of jND. All the Ins + jND experiments were carried out at pH 6.0 to facilitate the protein attachment. Figure 4a shows UV–vis absorption spectra of the Ins + jND supernatant from sample solutions in a series of insulin concentrations with fixed [jND] = 10 mg/mL. A 1.0 mg/mL insulin stock solution is also included to show the absorption band and peak position around 277 nm. The samples in the figure contain a concentration range of [Ins] = 0.5–10 mg/mL, corresponding to the Ins/jND number ratios of 0.5–10, respectively. At lower [Ins], free ND particles appear present in the supernatant, causing scattered light that is more sensitive toward the far UV region. Therefore, the signal intensity of [Ins] = 0.5 and 2.0 mg/mL is tilted higher in the lower wavelength region. As more insulin is added, the signal flattened out, eventually becoming indistinguishable from the baseline. Interestingly, no sign of free insulin can be found in the figure even at the highest [Ins] (10 mg/mL), where the number ratio reaches 10. The result is quite different from the Mb + jND and BSA + jND studies reported above where both free Mb and BSA are clearly present in supernatant when the jND surface is saturated. Apparently, eq 2 is not appropriate to describe the adsorption behavior here for insulin. Is this because insulin has not saturated the jND surface? Or, is it simply a different kind of surface attachment? To address this issue, we compare the result with the attachment of insulin to hND.

With [hND] fixed at 1.0 mg/mL, the samples containing [Ins] = 0.01–0.05 mg/mL give the number ratios of 6–30, respectively. Similar to the surface attachment on jND (Figure 4a), the spectra feature only free hND scattered light toward the far UV region, which decreases in increasing insulin concentration (data not shown). At [Ins] = 0.05 mg/mL, the amount of the scattered light becomes small enough that the signal intensity virtually merges in the spectrum baseline. At this concentration, most of hND particles are precipitated out

DOI: 10.1021/acs.jpca.5b01031
J. Phys. Chem. A XXXX, XXX, XXX–XXX

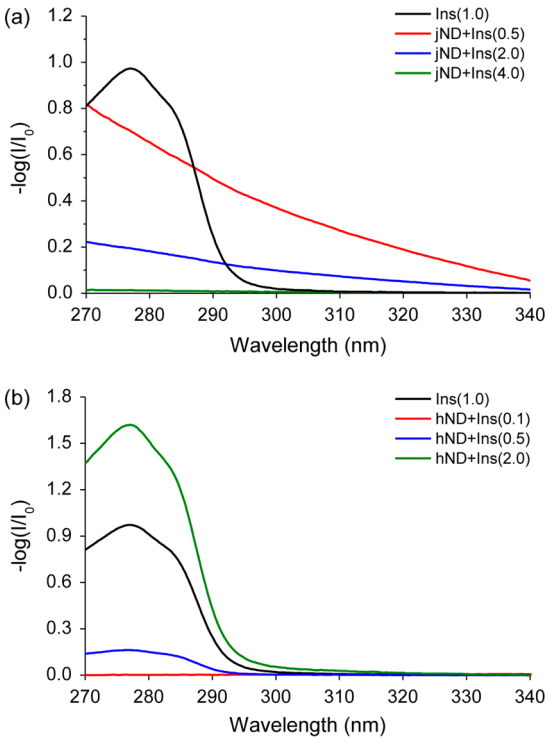

Figure 4. Comparison of UV−vis absorption spectra of (a) Ins stock (1.0 mg/mL) and Ins + jND supernatant at pH 6.0 and (b) Ins stock (1.0 mg/mL) and Ins + hND supernatant at pH 4.5. (See text.) The three featureless absorptions in (a) are due to light scattering from NDs at [Ins] = 0.5−4.0 mg/mL (numbers in parentheses) in 10 mg/mL jND. The absorptions at 280 nm in (b) are due to [Ins] = 0.1−2.0 mg/mL (numbers in parentheses) in 1.0 mg/mL hND. Appropriate dilution of the supernatant was made to obtain the spectra with $-\log(I/I_0) < 2$ in the measurement.

by insulin in some form of the Ins + hND complex, leaving no free hND in supernatant. With continued increase of the insulin concentration (Figure 4b), free insulin begins to appear in the supernatant. While no sign of insulin is observed at the least [Ins] (0.1 mg/mL) in this group of samples, a distinctive absorption band emerges at around 280 nm, as [Ins] grows to 0.5 mg/mL and more. The band matches perfectly both in the shape and peak position with the absorption of the insulin stock. Furthermore, the absorption band intensity increases when [Ins] raises in the supernatant, the same as in the cases of Mb + hND and BSA + hND.[14] In analogy to these two cases, beyond the surface saturation of hND, equilibrium is established between free and surface-bound insulin. At [Ins] = 0.5 mg/mL in Figure 4b, the surface is nearly saturated, and each 30 nm hND can accommodate up to 200 insulin molecules on its surface.

To explore further the difference in the adsorption behavior of insulin onto these two types of NDs, we look to mass spectrometry for clues. Figure 5a shows mass peaks obtained from Ins + hND prepared in 1.0 mg/mL of hND and 2.0 mg/mL of insulin at pH 4.5. The mass spectrum consists of a dominating peak at around 5800 and its dimer peak with intensity less than 1% of the monomer. At this concentration, the corresponding Ins/hND number ratio is 1200, which is well above the surface saturation estimated by UV−vis above. The data support the model of a monolayer coverage of insulin on hND. This surface attachment pattern is a result of the strong

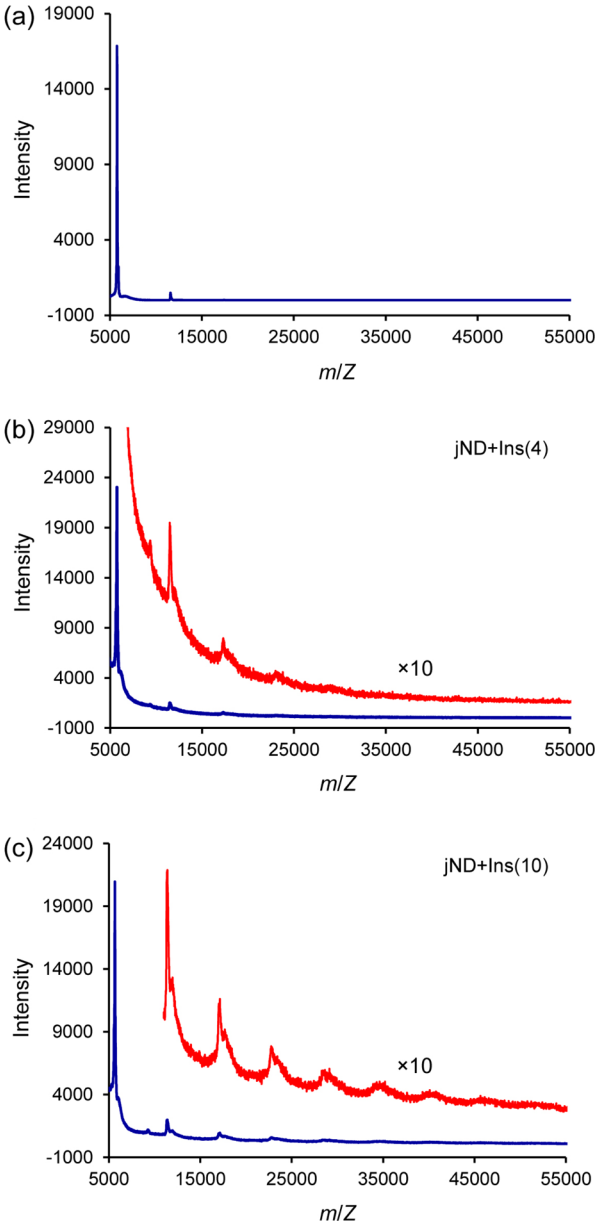

Figure 5. MALDI-TOF mass spectra of (a) Ins + hND prepared with [Ins] = 2.0 mg/mL in 1.0 mg/mL jND and (b and c) Ins + jND prepared with [Ins] = 4 and 10 mg/mL (numbers in parentheses), respectively, in 10 mg/mL jND at pH 6.0.

surface−protein interaction, which reduces the intermolecular protein−protein interaction upon adsorption.

Insulin attachment on jND has given mass spectra in Figure 5 (panels b and c). The two samples represent two different levels of insulin content: the lower [Ins] (4 mg/mL) in (b) and the higher [Ins] (10 mg/mL) in (c), both in [jND] = 10 mg/mL. Unlike that of hND, multiple peaks appear in both spectra, each corresponding to the mass of an Ins-multimer. In the expanded intensity scale of Figure 5b, the sample showed mass peaks up to 4 times the insulin molecular mass. Since the UV−vis spectra showed no free insulin absorption in the supernatant at this insulin concentration, aggregates of at least 4 insulin molecules must have existed on the surface of jND. The result is in agreement with our calculation for the Ins/jND number ratio of 4.5 at this concentration. Similarly, as the [Ins] was increased to 10 mg/mL, a progression of the mass peaks can be

DOI: 10.1021/acs.jpca.5b01031
J. Phys. Chem. A XXXX, XXX, XXX−XXX

easily identified up to 8 (Figure 5c). It suggests that all added insulin molecules are attached on the jND surface and, because of the strong protein−protein interaction, they are likely to attract each other together. Interestingly, the protein−protein attraction is strong enough to hold the insulin aggregates together through the laser-induced detachment and ionization process from jND.

The fact that not only can insulin grow in a large number on jND but also its stability is maintained and supports the model of insulin attachment on jND as

$$n\text{Ins} + \text{jND} \rightleftharpoons (\text{Ins})_n \cdot \text{jND} \quad (3)$$

In order to understand the formation of the insulin aggregates, we took a systematic approach in measuring the zeta potential of Ins + jND. Figure 6 displays a set of zeta

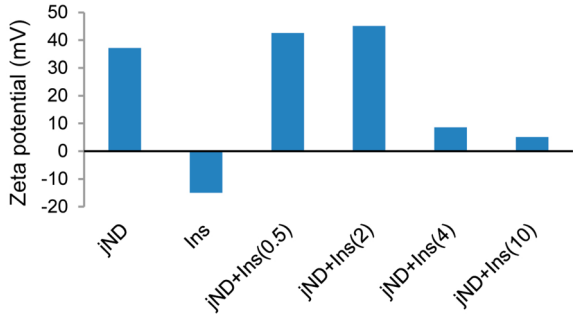

Figure 6. Zeta potential measurements of jND, Ins, and Ins + jND for [Ins] = 0.5−10 mg/mL (numbers in parentheses) in 10 mg/mL jND at pH 6.0.

potential measurements at [Ins] = 0−10 mg/mL with constant 10 mg/mL jND. Again, the high positive potential (+37 mV) of free jND prevents the particles from aggregation. Free insulin was measured at a negative potential, −15 mV, and when a small amount of insulin was first added, 0.5−2 mg/mL, the zeta potential was measured in the high +42 mV range, in favor of the Ins + jND complex at the nonaggregated state. As [Ins] increases to 4 mg/mL and above, the potential shows a dramatic decrease to +9 mV or less, indicating aggregation may have occurred that helps to stabilize the potential of the Ins + jND complex. This potential gap is coincident with the spectral result. When compared to UV−vis data (Figure 4a), the samples with high zeta-potential ([Ins] = 0.5−2 mg/mL) all correspond to spectral signals with significant scattered light. Free jND or positively changed $(\text{Ins})_n \cdot$jND particles are observed in supernatant. The low-potential samples ([Ins] = 4−10 mg/mL) give spectral signals well-aligned with the baseline in the figure, which have little or no scattered light. At this point, there is no free jND present in supernatant any more. All the NDs have become part of the Ins + jND complex aggregates in the precipitate, which is thermodynamically more stable than its free form in solution.

The question remains: what is the form of the insulin assembly on the surface? It is known that insulin in aqueous solution can exist as monomers, dimers, tetramers, and hexamers, depending on [Ins], solution pH, and the presence of other ions.[27] Aggregation of insulin also occurs at various interfaces.[28] In a kinetic study of insulin aggregation and fibrillation on a hydrophobic polystyrene surface, Smith et al.[29] reported a rapid formation of stable insulin aggregates at the initial stage of insulin growth, which was measured at a radius of 13 ± 1 nm. Additional Thioflavin-T fluorescence study was used to monitor β-sheet formation and their data show a significant amount of intermolecular β-sheets in the aggregates. As will be discussed in the following section, we have also found stable insulin multimers on ND that may follow the similar aggregation pattern. No insulin monomer attachment was ever observed in this work.

Desorption of Protein−ND. We now turn to the question of protein−ND structural configuration by investigating desorption of the protein−ND complex.

In the experiments, after centrifuging, supernatant of the sample solution was discarded and the precipitated nanodiamond with attached proteins were collected. The precipitate was washed and redissolved in buffer solution before being centrifuged again. The new supernatant, called "1st wash", was collected and analyzed by DLS measurement for the particle size. Therefore, any protein or nanodiamond present in the first wash must have come from the protein−ND precipitate (i.e., desorption from the protein−ND precipitate). These desorbed pieces are fragments falling off from the collective ND−protein complexes, which may be nanodiamond or free protein but also protein−ND complex that still bears resemblance to the precipitate. By studying these desorbed fragments, we hope to get further clues into the structural configuration of the protein−nanodiamond complex. In addition, by varying protein concentrations in the sample solution, and hence changing the protein surface coverage, it may also affect protein attachment on the nanodiamond. Therefore, it is reasonable to assume that the configuration of desorbed fragments from the protein−ND precipitate may be different as protein concentration is changed. The fragmentation pattern, if present, may lead to some understanding of the interactions between protein and nanodiamonds as discussed in the following sections.

Dynamic light scattering measurement data from the first wash for the three proteins + hND in this study are included in Table 1. The table consists of experimental measurement of the size (in diameter) of desorbed fragments in increasing protein concentrations, as well as the assignment of the particle numbers for protein and nanodiamonds in each desorbed fragment sample. Furthermore, each protein size in Table 1 is derived based on the assignment and the known hND size. A glance over data in Table 1 clearly reveals that the size distribution of desorbed fragments in all three proteins appears not random and all fragments are small in size. No large aggregates observed. In fact, the fragmentation shows a preference for specific combinations of proteins with nanodiamonds. Finally, no free proteins detected, even at the highest concentration reported in the table, which may have been caused by protein's loose structural density and hence low refractivity. It was observed in the experiment that adding ND would enhance detection sensitivity to a considerable extent in the DLS measurement.

The quantitative analysis starts with hND because of its large size and, hence, substantial contribution to the size measurement. Table 1 shows the first wash of hND with three proteins, each appears to have a rather specific measurement with a narrow range of size distribution. The average diameter is in the neighborhood of 70, 45, and 35 nm for BSA (pH 4), Ins (pH 4.5), and Mb (pH 5), respectively. Perhaps the most striking surprise from this table is that the size shows little or no change with the increasing of protein concentration, which is over a range as wide as 10-fold.

DOI: 10.1021/acs.jpca.5b01031
J. Phys. Chem. A XXXX, XXX, XXX−XXX

Table 1. DLS Size Measurement of Protein + hND

(protein, hND) (mg/mL)	diameter (nm)	hND number	protein number	diameter fit (nm)	protein (nm)
BSA + hND		hND = 30 nm			
					BSA
(1, 1)	69.4 ± 10.8	2	1.5	70.1	6.3
(2, 1)	73.3 ± 10.6	2	2	73.2	6.7
(5, 1)	74.0 ± 10.5	2	2	73.2	7.0
				avg =	6.6
				std =	0.4
				std% =	5.5%
Ins + hND		hND = 31 nm			
					Ins
(0.01, 1)	30 ± 5.2	1	0	31.0	
(0.025, 1)	44.2 ± 6.5	1	1	43.8	13.2
(0.05, 1)	44.2 ± 7.6	1	1	43.8	13.2
(0.1, 1)	43 ± 7.4	1	1	43.8	12.0
				avg =	12.8
				std =	0.7
				std% =	5.4%
Mb + hND		hND = 30.5 nm			
					Mb
(0.05, 2)	36.6 ± 6.4	1	1	36.2	6.1
(0.1, 2)	36.5 ± 6.5	1	1	36.2	6
(0.2, 1)	31.5 ± 5.5	1	0	30.5	
(0.3, 1)	41.7 ± 7.2	1	2	41.8	5.6
				avg =	5.9
				std =	0.3
				std% =	5.1%

The assignment of protein and nanodiamond numbers follows the model of the spherical topography of hND with the known average unit size, 30−31 nm, determined empirically. Therefore, the diameter in each DLS measurement other than nanodiamond must be contributed by protein. When the size of the desorbed fragment is small, involving only one or two hNDs, it is easy to assign each DLS measurement by a pair of protein and nanodiamond numbers. The resulting protein/hND number ratio may resemble the unit structure of the protein−hND complex. Following this logic, the three proteins are found to have protein/hND ratio of 2/2 (double pair) for BSA, 1/1 (single pair) for both Ins and Mb. The average size of each protein derived according to these data is BSA = 6.6, Ins = 12.8, and Mb = 5.9 (all diameter in nm), with a standard deviation of ∼5%. BSA is not a globular protein and, depending on which site is in contact with hND, the size measurements of BSA-hND may vary. As stated earlier, crystallography data of BSA indicate a molecular geometry averaging 4 × 4 × 14 nm. The average 6.6 ± 0.2 nm diameter measured in this work seems to be a reasonable representation of BSA attaching to hND at some tilt angle.

Table 1 displays a simple pattern in size measurement for Ins-hND over a 10-fold Ins concentration. The only two sizes observed, 30 or 44 nm, are attributed to hND and a single pair of Ins and hND, respectively. The fact that only one Ins-hND size is present exclusively throughout such a wide concentration range suggests an extraordinary stable Ins conformation, giving this Ins-multimer a derived diameter of 12.8 ± 0.4 nm. For a comparison, the crystal structure of 2 Zn Ins-hexamer shaped in an oblate geometry of 5 nm in diameter and 3.6 nm of height.[30] The stable Ins-multimer observed here has resulted from exceedingly strong protein−protein interactions that can hold up a sizable number of insulins together, probably even before attachment to hND. As discussed above in the Ins+ND attachment, this Ins-multimer may very well be a small insulin aggregate. Further study is needed for the structural details of the Ins-multimer and its stability.

Size measurements of Mb + hND from this work span a 6-fold Mb concentration range. Table 1 shows the number of Mb attached on hND ranging from 0 to 2, which may be increasing with Mb concentration. The derived Mb size is 5.9 ± 0.3 nm in diameter, which is larger than the average of its globular structure of 2.5 × 3.5 × 4.5 nm. There may be a slight adjustment in Mb conformation upon attachment to hND. Because of hND's relatively large size, and its ample surface available for protein attachment, our DLS data clearly show that the surface coverage is monolayer. Desorbed fragments reported in Table 1 are all in single units of one hND and one Mb, until reaching the highest [Mb] sample where the surface becomes oversaturated. The tendency for the Mb + hND complex to form single units is a confirmation of a strong protein−surface interaction, perhaps at the expense of weakening protein−protein attraction.

Analyzing desorption data from the jND surface poses additional challenges. Unlike hND, whose assignment can be unambiguously made, jND is either compatible or smaller than the proteins tested in this work. Protein attachment can no longer be treated as adsorption on a two-dimensional surface. Instead, it must be considered conformational interaction involving structural geometry of the nanodiamond. The assignments can no longer be made uniquely using DLS data alone, further study will be needed for verification.

CONCLUSION

This work surveys the surface attachment of three proteins (Mb, BSA, and Ins) of different sizes, molecular mass, conformation, and biological functions with two kinds of NDs: positively charged jND and negatively charged hND. The study clearly reveals a significant difference in binding affinity between these two NDs for proteins. The monocrystalline hND, with its strong protein−surface interaction with all three proteins, favors monolayer protein coverage, similar to a thin film on the particle surface. The detonated jND, on the other hand, shows a significantly less protein−surface interaction with the proteins. Because of the small size of the diamond nanoparticles (only ∼4 nm), both the Mb and BSA form 1:1 complexes with the jND at saturation. Insulin has strong intermolecular bonding and forms stable multimers of 13 nm in diameter on the ND surface. Both NDs have great potential to serve as biocompatible vehicles for drug delivery in biology and nanoscale medicine.

ASSOCIATED CONTENT

Supporting Information

Additional data of Mb attachment on hND. This material is available free of charge via the Internet at http://pubs.acs.org.

AUTHOR INFORMATION

Corresponding Authors

*E-mail: hchang@gate.sinica.edu.tw. Tel: 886-2-2366-8260.
*E-mail: sum@sonoma.edu. Tel: 707-664-4057.

DOI: 10.1021/acs.jpca.5b01031
J. Phys. Chem. A XXXX, XXX, XXX−XXX

Notes

The authors declare no competing financial interest.

■ ACKNOWLEDGMENTS

This work is supported by Academia Sinica and Ministry of Science and Technology, Taiwan, with Grant 103-2628-M-001-005. M.-C.S. acknowledged Academia Sinica for granting the opportunity to carry out this project in Taipei.

■ REFERENCES

(1) Davis, M. E.; Chen, Z. G.; Shin, D. M. Nanoparticle Therapeutics: An Emerging Treatment Modality for Cancer. *Nat. Rev. Drug Discovery* **2008**, *7*, 771−782.
(2) Peer, D.; Karp, J. M.; Hong, S.; Farokhzad, O. C.; Margalit, R.; Langer, R. Nanocarriers as an Emerging Platform for Cancer Therapy. *Nat. Nanotechnol.* **2007**, *2*, 751−760.
(3) Jensen, A. W.; Wilson, S. R.; Schuster, D. I. Biological Applications of Fullerenes. *Bioorg. Med. Chem.* **1996**, *4*, 767−779.
(4) Lacerda, L.; Bianco, A.; Prato, M.; Kostarelos, K. Carbon Nanotubes as Nanomedicines: From Toxicology to Pharmacology. *Adv. Drug Delivery Rev.* **2006**, *58*, 1460−1470.
(5) Bitounis, D.; Ali-Boucetta, H.; Hong, B. H.; Min, D.-H.; Kostarelos, K. Prospects and Challenges of Graphene in Biomedical Applications. *Adv. Mater.* **2013**, *25*, 2258−2268.
(6) Vaijayanthimala, V.; Chang, H.-C. Functionalized Fluorescent Nanodiamonds for Biomedical Applications. *Nanomedicine* **2009**, *4*, 47−55.
(7) Xing, Y.; Dai, L. M. Nanodiamonds for Nanomedicine. *Nanomedicine* **2009**, *4*, 207−218.
(8) Schrand, A. M.; Johnson, J.; Dai, L.; Hussain, S. M.; Schlager, J. J.; Zhu, L.; Hong, Y.; Osawa, E. In: Webster, T. J. *Safety of Nanoparticles*. Springer: New York, 2009; pp 159−187.
(9) Lam, R.; Ho, D. Nanodiamonds as Vehicles for Systemic and Localized Drug Delivery. *Expert Opin. Drug Delivery* **2009**, *6*, 883−895.
(10) Hui, Y. Y.; Chang, C.-L.; Chang, H.-C. Nanodiamonds for Optical Bioimaging. *J. Phys. D: Appl. Phys.* **2010**, *43*, 374021.
(11) Schirhagl, R.; Chang, K.; Loretz, M.; Degen, C. L. Nitrogen-Vacancy Centers in Diamond: Nanoscale Sensors for Physics and Biology. *Annu. Rev. Phys. Chem.* **2014**, *65*, 83−105.
(12) Mochalin, V. N.; Shenderova, O.; Ho, D.; Gogotsi, Y. The Properties and Applications of Nanodiamonds. *Nat. Nanotechnol.* **2012**, *7*, 11−23.
(13) Osawa, E. Monodisperse Single Nanodiamond Particles. *Pure Appl. Chem.* **2008**, *80*, 1365−1379.
(14) Kong, X. L.; Huang, L. C. L.; Hsu, C.-M.; Chen, W.-H.; Han, C.-C.; Chang, H.-C. High-Affinity Capture of Proteins by Diamond Nanoparticles for Mass Spectrometric Analysis. *Anal. Chem.* **2005**, *77*, 259−265.
(15) Chen, W.-H.; Lee, S.-C.; Sabu, S.; Fang, H.-C.; Chung, S.-C.; Han, C.-C.; Chang, H.-C. Solid-Phase Extraction and Elution on Diamond (SPEED): A Fast and General Platform for Proteome Analysis with Mass Spectrometry. *Anal. Chem.* **2006**, *78*, 4228−4234.
(16) Tzeng, Y.-K.; Faklaris, O.; Chang, B.-M.; Kuo, Y.; Hsu, J. H.; Chang, H.-C. Superresolution Imaging of Albumin-Conjugated Fluorescent Nanodiamonds in Cells by Stimulated Emission Depletion. *Angew. Chem., Int. Ed.* **2011**, *50*, 2262−2265.
(17) Shimkunas, R. A.; Robinson, E.; Lam, R.; Lu, S.; Xu, X.; Zhang, X. Q.; Huang, H.; Osawa, E.; Ho, D. Nanodiamond-Insulin Complexes as pH-Dependent Protein Delivery Vehicles. *Biomaterials* **2009**, *30*, 5720−5728.
(18) Smith, A. H.; Robinson, E. M.; Zhang, X. Q.; Chow, E. K.; Lin, Y.; Osawa, E.; Xi, J.; Ho, D. Triggered Release of Therapeutic Antibodies from Nanodiamond Complexes. *Nanoscale* **2011**, *3*, 2844−2848.
(19) Huang, L.-C.; Chang, H.-C. Adsorption and Immobilization of Cytochrome c on Nanodiamonds. *Langmuir* **2004**, *20*, 5879−5884.
(20) Chung, P.-H.; Perevedentseva, E.; Tu, J.-S.; Chang, C. C.; Cheng, C.-L. Spectroscopic Study of Bio-Functionalized Nanodiamonds. *Diamond Relat. Mater.* **2006**, *15*, 622−625.
(21) Wang, H.-D.; Niu, C. H.; Yang, Q.; Badea, I. Study on Protein Cnformation and Adsorption Behaviors in Nanodiamond Particle-Protein Complexes. *Nanotechnology* **2011**, *22*, 145703−145713.
(22) Osawa, E. Recent Progress and Perspectives in Single-Digit Nanodiamond. *Diamond Relat. Mater.* **2007**, *16*, 2018−2022.
(23) Li, H.-C.; Hsieh, F.-J.; Chen, C.-P.; Chang, M.-Y.; Hsieh, P. C. H.; Chen, C.-C.; Hung, S.-U.; Wu, C.-C.; Chang, H.-C. The Hemocompatibility of Oxidized Diamond Nanocrystals for Biomedical Applications. *Sci. Rep.* **2013**, *3*, 3044.
(24) Blackstock, J. C. *Guide to Biochemistry*; John Wright: London, 1989.
(25) Peter, T., Jr. Serum Albumin. *Adv. Protein Chem.* **1985**, *37*, 161−245.
(26) Bohren, C. F.; Huffman, D. R. *Absorption and Scattering of Light by Small Particles*; Wiley: New York, 1983.
(27) Blundell, T. L.; Dodson, G. G.; Hodgkin, D. C.; Mercola, D. A. Insulin: The Structure in the Crystal and its Reflection in Chemistry and Biology. *Adv. Protein Chem.* **1972**, *26*, 279−402.
(28) Li, S.; Leblanc, R. M. Aggregation of Insulin at the Interface. *J. Phys. Chem. B* **2014**, *118*, 1181−1188.
(29) Smith, M. I.; Sharp, J. S.; Roberts, C. J. Nucleation and Growth of Insulin Fibrils in Bulk Solution and at Hydrophobic Polystyrene Surfaces. *Biophys. J.* **2007**, *93*, 2143−2151.
(30) Hvidt, S. Insulin Association in Neutral Solutions Studied by Light Scattering. *Biophys. Chem.* **1991**, *39*, 205−213.

DOI: 10.1021/acs.jpca.5b01031
J. Phys. Chem. A XXXX, XXX, XXX−XXX